WO_x/TiO_2 Catalysts via Titania Nanotubes for the Oxidation of Dibenzothiophene

M.A. Cortes-Jácome, M. Morales, C. Angeles Chavez, L.F. Ramírez-Verduzco, E. López-Salinas, and J.A. Toledo-Antonio*

Instituto Mexicano del Petróleo, Eje Central Lázaro Cárdenas # 152, 07730 México D.F., México

Received July 25, 2007. Revised Manuscript Received September 26, 2007

WO_x/TiO_2 catalysts were synthesized by impregnating aqueous $(NH_4)_2WO_4$ on hydrous titania nanotubes. The materials were annealed in air at 500 °C and characterized by X-ray diffraction (XRD), Raman spectroscopy, high-resolution transmission electron microscopy (HRTEM), high-angle annular dark-field scanning transmission electron microscopy (HAADF-STEM), and X-ray photoelectron spectroscopy (XPS); their catalytic activity was evaluated in the oxidation reaction of dibenzothiophene (DBT). After annealing at 500 °C, the structure of the support transformed from orthorhombic, with nanotubular morphology, to tetragonal, yielding anatase nanoparticles decorated by tungsten nanoparticles on its surface. During this transformation, the nanotubes released residual Na^+ ions from the interlayer space, which reacted with tungstate species to change the W coordination from octahedral to tetrahedral, yielding ≤ 1 nm $Na_x(WO_4)$ nanoparticles on the surface of anatase TiO_2. These nanoparticles were highly active for the DBT oxidation, showing a linear dependence on the W surface density at concentrations below 6.9 W/nm^2. In TiO_2 oversaturated with tungsten nanoparticles, the intrinsic kinetic velocity (r_{DBT}) of the DBT oxidation reached its maximum value; 6.9 W /nm^2 is then the optimum surface density concentration to attain a high catalytic activity in the DBT oxidation.

1. Introduction

Tungsten oxide loaded on different supports, such as Al_2O_3, SiO_2, ZrO_2, and TiO_2, are known to be catalytically active for several reactions, including alcohol dehydrogenation, *n*-alkane isomerization, oxidative desulphurization (ODS), and cracking and alkylation of hydrocarbons.[1–10] A common characteristic of these catalysts is their high acidity, being able to catalyze the isomerization reactions at low temperatures, wherein the formation of branched alkanes are thermodynamically favored.[11,12] The most active catalysts have been prepared on ZrO_2, and hence, they have been the most extensively studied.[12–20] High temperature (>700 °C) is required for activating catalytic sites on WO_3-ZrO_2 systems, by expelling the WO_3 species onto the zirconia surface.[16,21–24] Accordingly, the WO_x surface density attained was around 7 W/nm^2, the optimum value for monolayer coverage, where the material develops optimum acidity and catalytic activity in several reactions.[15,25,26] By an HRTEM study, we have identified nanoclusters of WO_x domains having a size of 0.5−3.0 nm that are smeared on the ZrO_2 surface,[27–29] promoting acidity and catalytic activity in isomerization reactions.[29]

* Corresponding author. E-mail: jtoledo@imp.mx.

(1) Hino, M.; Arata, K. *J. Chem. Soc., Chem Commun* **1987**, 1259.
(2) Yamaguchi, T. *Appl. Catal., A* **1990**, *6*, 1.
(3) Ramis, G.; Cristiani, C.; Leitti, L.; Forzatti, P.; Bregani, F. *Langmuir* **1992**, *8*, 1744.
(4) Baertsch, C. D.; Komala, K. T.; Chua, Y. H.; Iglesia, E. *J. Catal.* **2002**, *205*, 44.
(5) Kim, T.; Burrows, A.; Kiely, C. J.; Wachs, I. E. *J. Catal.* **2007**, *246*, 370.
(6) Macht, J.; Baertsch, C. D.; May-Lozano, M.; Soled, S. L.; Wang, Y.; Iglesia, E. *J. Catal.* **2004**, *227*, 479.
(7) Sarish, S.; Devassy, B. M.; Böhringer, W.; Fletcher, J.; Halligudi, S. B. *J. Mol. Catal. A: Chem.* **2005**, *240*, 123.
(8) Di-Grégorio, F.; Keller, V.; Di-Costanzo, T.; Vignes, J. L.; Michel, D.; Maire, G *Appl. Catal., A* **2001**, *218*, 13.
(9) Xiao, X.; Tierney, J. W.; Wender, I. *Appl. Catal., A* **1999**, *183*, 209.
(10) Eibl, S.; Jentoft, R. E.; Gates, B. C.; Knözinger, H. *Phys. Chem. Chem. Phys.* **2000**, *2*, 2565.
(11) Iglesia, E.; Barton, D. G.; Soled, S. L.; Miseo, S.; Baumgartner, J. E.; Gates, W. E.; Fuentes, G. A.; Meitzner, G. D. *Surf. Sci. Catal.* **1996**, *101*, 533.
(12) Santiesteban, J. G.; Vartuli, J. C.; Han, S.; Bastian, D.; Chang, C. D. *J. Catal.* **1997**, *168*, 431.
(13) Scheithauer, M.; Cheung, T. K.; Jentoft, R. E.; Grasselli, R. K.; Gates, B. C.; Knözinger, H. *J. Catal.* **1998**, *180*, 1.
(14) Xie, S.; Chen, K.; Bell, A. T.; Iglesia, E. *J. Phys. Chem. B* **2000**, *104*, 10059.
(15) Barton, D.; Soled, S. L.; Meitzner, G. D.; Fuentes, G. A.; Iglesia, E. *J. Catal.* **1999**, *181*, 57.
(16) Cordischi, D.; Occhiuzzi, M.; Dragone, R. *J. Solid State Chem.* **1998**, *136*, 263.
(17) Bokhimi, X.; Morales, A.; García, A.; Xiao, T. D.; Chen, H.; Strutt, P. R. *J. Solid State Chem.* **1999**, *142*, 409.
(18) Baertsch, C. D.; Soled, S.; Iglesia, E *J. Phys. Chem.* **2001**, *105*, 1329.
(19) Ward, D. A.; Ko, E. I. *J. Catal.* **1994**, *150*, 18.
(20) Triwahyono, S.; Yamada, T.; Hattori, H. *Appl. Catal., A* **2003**, *250*, 75.
(21) Afanasiev, P.; Geantet, C.; Breysse, M.; Coudurier, G.; Vedrine, J. C. *J. Chem. Soc., Faraday Trans,* **1994**, *90*, 193.
(22) Boyse, R. A.; Ko, E. I. *J. Catal.* **1997**, *171*, 191.
(23) Boyse, R. A.; Ko, E. *J. Catal.* **1998**, *179*, 100.
(24) Boyse, R. A.; Ko, E. *Catal. Lett.* **1996**, *38*, 225.
(25) Barton, D. G.; Shtein, M.; Wilson, R. D.; Soled, S. L.; Iglesia, E. *J. Phys.Chem. B* **1999**, *103*, 630.
(26) Iglesia, E.; Barton, D. G.; Biscardi, J. A.; Guines, M. J. L.; Soled, S. L. *Catal. Today* **1997**, *38*, 339.
(27) Angeles-Chavez, C.; Cortés-Jacome, M. A.; Torres, E.; Toledo, J. A. *J. Mater. Res.* **2006**, *21*, 807.
(28) Cortes-Jacome, M. A.; Angeles-Chavez, C.; Bokhimi, X.; Toledo, J. A. *J. Solid State Chem.* **2006**, *179*, 2663.
(29) Cortes-Jacome, M. A.; Angeles-Chavez, C.; Bokhimi, X.; Toledo, J. A. *Appl. Catal., A* **2007**, *318*, 178.

10.1021/cm702010k CCC: $37.00
Published on Web 11/20/2007

Table 1. Textural Properties and W Concentration after Annealing at 500 °C

sample	SSA (m^2/g)	total pore volume (cm^3/g)	avg. pore diameter (nm)	W(nominal) (wt %)	W(real) (wt %)	surface density (W/nm^2)
NT[a]	310	0.61	6.5	0.0	0.0	0.0
NT support[b]	257	0.60	7.2	0.0	0.0	0.0
NTW-05	80	0.41	17	5.0	3.8	1.6
NTW-10	72	0.32	15	10.0	7.6	3.8
NTW-15	71	0.38	18	15.0	12.9	6.9
NTW-20	68	0.33	15	20.0	18.0	10.6
NTW-20[c]	210	0.44	6.9	20.0	18.0	3.4
WO_x/Al_2O_3	228	0.50	6.6	17.8	n.d.[d]	3.1

[a] Dried NT support, outgassed at 100 °C. [b] NT support annealed at 400 °C. [c] Tungstated sample annealed at 400 °C. [d] n.d. = not determined.

Particularly, tungstated zirconia catalysts have shown good ODS activity on organic sulfur compounds. In this reaction, the sulfur compounds are usually transformed into the corresponding sulfone compounds with an oxidant agent, such as H_2O_2, organic hydroperoxides or peroxyacids, ozone, etc.[30] Because sulfur specification in diesel and gasoline became recently more stringent, this approach of desulphurization of liquid fuels has regained an interest and many reports have appeared in literature.[30–35] Accordingly, tetrahedrally coordinated W atoms bonded to the ZrO_2 surface are more active W species than octahedrally coordinated ones in WO_3 nanoparticles.[36] W atoms in tetrahedral environment have been incorporated into the interlayer space of Mg−Al layered double hydroxides, yielding highly active catalysts for ODS reaction.[37] More recently, Na_2WO_4 dissolved in the reaction media by adding an acetic acid solution were found to be highly efficient at transforming organic sulfur compounds contained in a commercial diesel into their corresponding sulfones.[38]

On the other hand, Hulea et al.[39–42] have reported that titanium incorporated into microporous materials, such as zeolites, (Ti-ZSM-12, Ti-Beta, TS-1) and MCM-type mesoporous titano-silicates (Ti-MCM-41, Ti-HMS) efficiently oxidize different organic substrates such as olefins, phenols, alcohols, thioethers, and sulfoxides using H_2O_2 or tert-butylhydroperoxide as oxidants.[40] However, the microporosity of these systems limits their application in the oxidation of large molecules, such as aromatic sulfur compounds contained in diesel fuel. Corma et al. demonstrated that Ti-MCM-41, with a larger pore size than zeolites (i.e., ∼4.0 nm) is able to desulfurize diesel in a continuous fixed bed reactor with high catalytic activity and long lifetime, making it possible to think in an industrial scale up of the ODS approach to achieve ultra low sulfur diesel by a more economical pathway.[43]

To the best of our knowledge, WO_x−TiO_2 has not been reported as a catalyst for ODS. In this context, anatase titanium oxide has been converted into titania nanotubes or nanofibers through a relatively simple alkaline hydrothermal method,[44,45] representing a suitable methodology for rapid manufacturing scale-up. The nanotubes exhibit large internal and external surfaces, along with surface in the vertex and

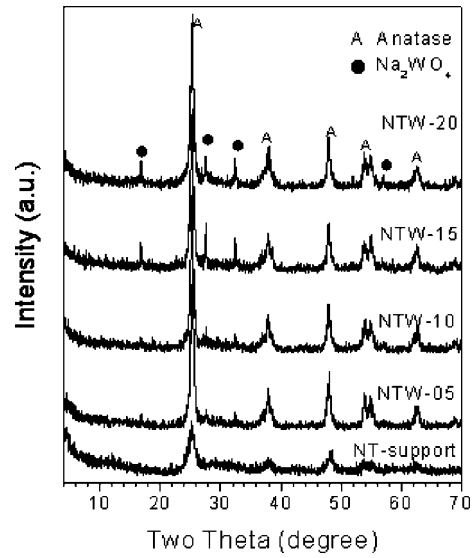

Figure 1. XRD patterns of NT support and derived tungstated titania calcined at 500 °C.

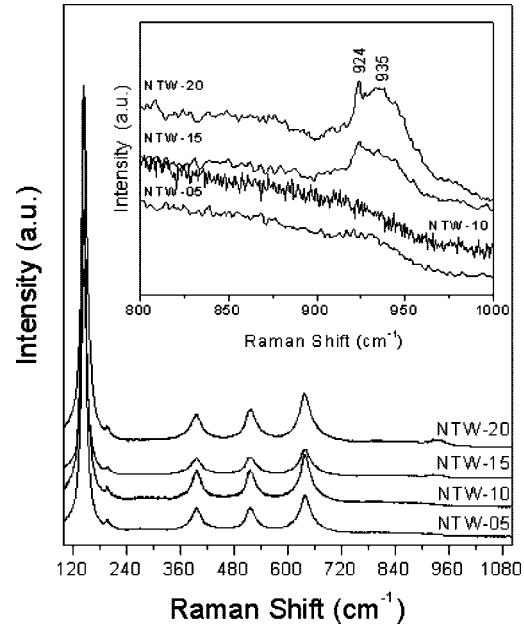

Figure 2. Raman spectra of tungstated titania catalysts. Inset: Magnification of tungstate vibrating region.

(30) Ito, E. Rob van Veen. J.A. *Catal. Today* **2006**, *116*, 446.
(31) Palomeque, J.; Clacens, J. M.; Figueras, F. *J. Catal.* **2002**, *211*, 103.
(32) Dimitriu, E.; Guimon, C.; Cordoneanu, A.; Casenave, S.; Hulea, T.; Chelaru, C.; Martinez, H.; Hulea, V. *Catal. Today* **2001**, *66*, 529.
(33) Cedeño-Caero, L.; Hernandez, E.; Pedraza, F.; Murrieta, F. *Catal. Today* **2005**, *564*, 107.
(34) Torres-García, E.; Canizal, G.; Velumani, S.; Ramirez-Verduzco, L. F.; Murrieta-Guevara, F.; Ascencio, J. A. *Appl. Phys. A: Mater. Sci. Process.* **2004**, *79*, 2037.
(35) Ramirez Verduzco, L. F.; Torres-Garcia, E.; Gomez-Quintana, R.; Gonzalez -Peña, V.; Murrieta -Guevara, F. *Catal. Today* **2004**, *98*, 289.
(36) Figueras, F.; Palomeque, J.; Loridant, S.; Fèche, C.; Essayem, N.; Gelbard, G. *J. Catal.* **2004**, *226*, 25.
(37) Hulea, V.; Maciuca, A. L.; Fajula, F.; Dimitriu, E. *Appl. Catal., A* **2006**, *313*, 200.
(38) Al-Shahrane, F.; Xiao, T.; Llewellyn, S. A.; Barri, S.; Jiang, Z.; Shi, H.; Martinie, G.; Green, M. L. H. *Appl. Catal., B* **2007**, *73*, 311.
(39) Moreau, P.; Hulea, V.; Gomez, S.; Brunel, D.; Di-Renzo, F. *Appl. Catal., A* **1997**, *155*, 253.
(40) Hulea, V.; Dumitriu, E.; Patcas, F.; Popot, R.; Graffin, P.; Moreau, P. *Appl. Catal., A* **1998**, *170*, 169.
(41) Hulea, V.; Dimitriu, E. *Appl. Catal., A* **2004**, *277*, 99.
(42) Hulea, V.; Fajula, F.; Bousquet, J. *J. Catal.* **2001**, *198*, 179.
(43) Chica, A.; Corma, A.; Domine, M. E. *J. Catal.* **2006**, *242*, 299.

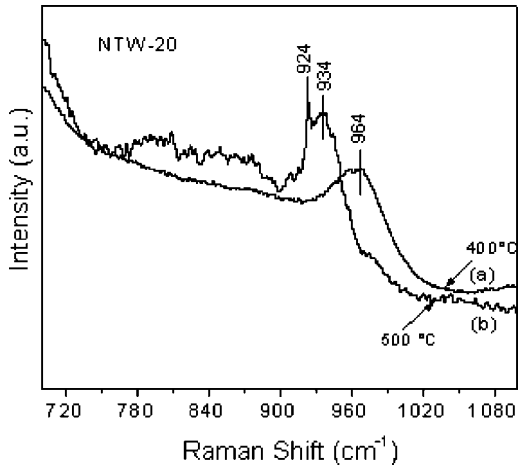

Figure 3. Raman spectra of NTW-20 sample at room temperature after annealing at (a) 400 and (b) 500 °C.

surface in the interlayer regions that compose the nanotube walls.[46,47] In fact, the transformation of titania into nanotubes yields materials with specific surface area as large as 400 m^2/g,[48] with inner diameters around 7 nm, opening new possibilities of applications for this kind of materials to oxidize large molecules or as support of transition metal oxides or sulfides. Recently, we have reported that CoMoS/nanostructured titania, i.e., sulfided cobalt-molybdenum on titania nanotubes, are very active in dibenzothiophene hydrodesulphurization.[49,50]

In this work, we use nanotubular titania (NT) as a precursor of anatase to support WO_x species. Initial advantages of NT, such as (*i*) high specific surface area, (*ii*) unconventional surface topography (e.g., uniformly curved surfaces and tube mouth edges), and (*iii*) confinement effects within the tubes, are very attractive for exploitation as catalysts or as a precursor of catalysts. Additionally, the solid-state reaction of NT and WO_x species upon a thermal treatment may result in an interesting material. On the one hand, single NTs transform into anatase nanoparticles above 400 °C; on the other hand, $(WO_4)^{2-}$ anions when incorporated in hydrous supports like zirconia hinder their crystal phase transformation. These two competing effects are used in this work as an attempt to obtain active WO_x-TiO_2 catalysts for the oxidation of DBT.

2. Experimental Section

2.1. Preparation of Catalysts. Titania nanotubes were synthesized by an alkali hydrothermal treatment of an anatase precursor with a crystallite size of 8.0 nm following the procedure published elsewere.[51] The starting support dried at 100 °C had a specific surface area of 310 m^2/g, pore volume of 0.61 cm^3/g, and average pore diameter of 6.5 nm. The residual amount of Na^+ ions contained in the nanotubular support was about 2.0 wt %, as determined by energy-dispersive X-ray spectroscopy (EDXS). Twenty-three grams of the support was impregnated with 200 cm^3 of an ammonium metatungstate solution at variable concentration to obtain 5, 10, 15, and 20 wt % W on the final product. The pH of the solution was adjusted to 10 with a few drops of ammonium hydroxide. The slurry was aged 1 h at room temperature and then excess water was eliminated by evaporation at 100 °C in a rotary evaporator. Finally, the sample was dried overnight at 110 °C and then calcined at 500 °C in an air flow for 4 h. Samples were labeled as NTW-*x*, where *x* represent the nominal wt % W amount. A fraction of the sample NTW-20, with the largest nominal W content (e.g., 20 wt %) was calcined at 400 °C, in order to preserve the nanotubular morphology. As reference, a commercial alumina was impregnated with 17.8 wt % of tungsten following the same procedure and annealed at 500 °C in air for 4 h.

2.2. Characterization Techniques. X-ray diffraction (XRD) patterns of the samples, packed in a glass holder, were recorded at room temperature with Cu $K\alpha$ radiation in a Bruker Advance D-8 diffractometer having theta−theta configuration and a graphite secondary-beam monochromator. The diffraction intensity was measured in the 2θ range between 15 and 110°, with a 2θ step of 0.02° for 8 s per point.

Real W concentration was quantified on samples annealed at 500 °C by atomic absorption spectroscopy (AAS) in a Perkin-Elmer 5000 spectrophotometer.

Textural properties were determined in an ASAP-2000 analyzer from Micromeritics. Specific surface area (SSA) was calculated from N_2 physisorption at –196 °C using the Brunauer−Emmet−Teller (BET) equation. Pore size distribution was obtained by the Barrett–Joyner–Halenda (BJH) method in the desorption stage. Dried samples were outgassed at 100 °C and those calcined at 400 °C were outgassed at 350 °C.

The Raman spectra were recorded using a Jobin Yvon Horiba (T64000) spectrometer, equipped with a confocal microscope (Olympus, BX41) with an argon ion laser operating at 514.5 nm at a power level of 10 mW. The spectrometer was equipped with a CCD camera detector.

X-ray photoelectron spectroscopy (XPS) spectra were recorded on a THERMO-VG SCALAB 250 spectrometer equipped with Al Kα X-ray source (1486.6 eV) and a hemispherical analyzer. The base pressure during the analysis was 1.37×10^{-7} Pa. The XPS analyses were performed in a static system on the samples, after ex situ calcination procedure. The experimental peaks were decomposed into components using mixed Gaussian–Lorentzian functions, nonlinear squares fitting algorithm, and Shirley-type background subtraction by using XPS peak fit software. The C_{1s} line at 284.6 eV was used as an internal standard for the correction of binding energies (BE). Changes in the W(4f) + Ti(3p) signal shape on the samples calcined at different temperatures were analyzed by a curve fitting procedure with doublets endowed with fixed spectroscopic parameters, but using variable position, full width at half-maximum (fwhm), and intensities. The spectroscopic parameters used were adopted from literature,[52] that is, $W(4f_{7/2}) - W(4f_{5/2})$ spin–orbit separation of 2.1 eV and intensity ratio $R = 0.75$. Surface elemental composition was determined by fitting and

(44) Kasuga, T.; Hiramatsu, M.; Hoson, A.; Sekino, T.; Niihara, K. *Langmuir* **1998**, *14*, 3160.
(45) Du, G. H.; Chen, Q.; Che, R. C.; Yuan, Z. Y.; Peng, L. M. *Appl. Phys. Lett.* **2001**, *79*, 3702.
(46) Tenne, R. *Nature* **2004**, *431*, 640.
(47) Tenne, R. *Angew. Chem., Int. Ed.* **2003**, *42*, 5124.
(48) Cheng, C.; Teng, H. *Chem. Mater.* **2004**, *16*, 4352.
(49) Escobar, J.; Toledo, J. A.; Cortés, M. A.; Mosqueira, M. L.; Perez, V.; Ferrat, G.; López Salinas, E.; Torres, E. *Catal. Today* **2005**, *106*, 222.
(50) Cortés-Jácome, M. A.; Escobar, J.; Angeles Chávez, C.; López Salinas, E.; Romero, E.; Ferrat, G.; Toledo-Antonio, J. A. *Catal. Today*, **2007**, doi:10.1016/j.cattod.2007.07.012.
(51) Cortés-Jácome, M. A.; Ferrat-Torres, G.; Flores Ortiz, L. F.; Angeles-Chávez, C.; López-Salinas, E.; Escobar, J.; Mosqueira, M. L.; Toledo-Antonio, J. A. *Catal. Today* **2007**, *126*, 248.
(52) Occhiuzzi, M.; Cordischi, D.; Gazzolli, D.; Valigi, M.; Heydorn, P. *Appl. Catal., A* **2004**, *269*, 169.

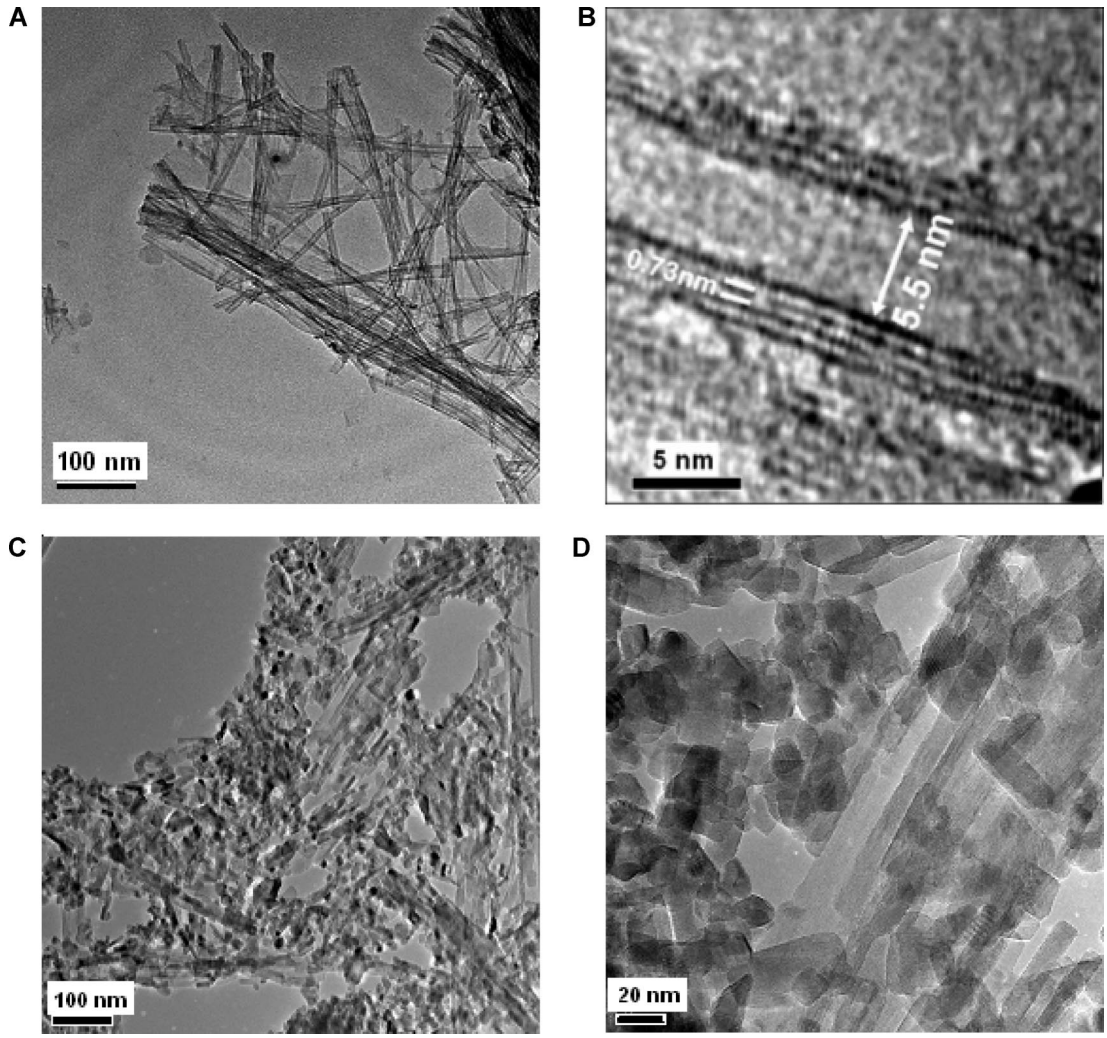

Figure 4. (a) TEM image of dried nanotubular support, (b) high-resolution TEM image of a single nanotube on NT support showing interlayer spacing of nanotubular walls and inner diameter, (c) TEM images of NTW-20 catalyst after calcination at 500 °C, and (d) high-magnification image of NTW-20 after annealing at 500 °C.

integrating the W_{4f}, $Ti_{2p,}$ C_{1s}, O_{1s}, and Na_{1s} bands and converting these values to atomic ratios using theoretical sensitivity factors provided by the manufacturer of the XPS apparatus.[53]

Transmission electron microscopy (TEM) and scanning transmission electron microscopy (STEM) were performed in a JEM-2200FS microscope with accelerating voltage of 200 kV. The microscope is equipped with a Schottky-type field emission gun and an ultrahigh resolution (UHR) configuration (Cs = 0.5 mm; Cc = 1.1 mm; point-to-point resolution = 0.19 nm) and in-column omega-type energy filter. STEM is particularly useful in nanoparticles studies by using a high-angle annular dark field (HAADF) detector, which collects electrons that undergo Rutherford scattering; thus the image can be acquired where the intensity is approximately proportional to Z^2 (Z being the atomic number of the scattering atom). Therefore, elements with a high Z show higher intensities and a white contrast in the image. This technique is useful for distinguishing the presence of different chemical elements when there is a big difference in the atomic number among them, such as supported catalysts.

Local chemical analysis by energy-dispersive X-ray spectroscopy (EDXS) was performed in a NORAN energy-dispersive X-ray spectroscope, which is attached to the microscope using the STEM-EDX combination. The samples were ground, suspended in 2-propanol at room temperature, and dispersed with ultrasonic agitation; an aliquot of the solution was then dropped on a 3 mm diameter lacey carbon copper grid.

2.3. Catalytic Tests. The oxidation of DBT by hydrogen peroxide was studied in a Robinson−Mahoney glass reactor under stirring at 2200 rpm and atmospheric pressure. A heated circulating bath was used to control temperature at 60 °C. In a typical experiment, 150 mL of γ-butyrolactone as solvent, 8 mL of hydrogen peroxide (30 wt %) as oxidant, and 0.075 g of catalyst were introduced when the thermal equilibrium was reached. The initial concentration of DBT was 4.6×10^{-5} mol/cm^3. The experimental conditions were carefully chosen so that the intrinsic reaction domain avoided the external diffusion regime. The progress of the reaction was followed by gas chromatography using an Alltech Econocapillary column (5% phenyl-95% methylpolysiloxane, 30 m × 0.25 m i.d., 250 μm film thickness). A quantitative analysis was performed by the internal standard method where sulfolane was used.

The apparent kinetic constants (k_{app}) were calculated assuming a pseudofirst order reaction. A plot of $(V_{solv}/m_{cat})(-\ln (C_{DBT}/C_{DBT}, \text{initial}))$ versus t was performed in order to obtain the slope that represents the k_{app}. The turnover rate (TOR) was calculated by normalizing the oxidation reaction rates to the total number of W atoms determined by AAS.

(53) *XPS and Auger Handbook*;Doc. Number: 600001; Thermo VG Scientific: West Sussex, U.K., 2003; Vol. 2.

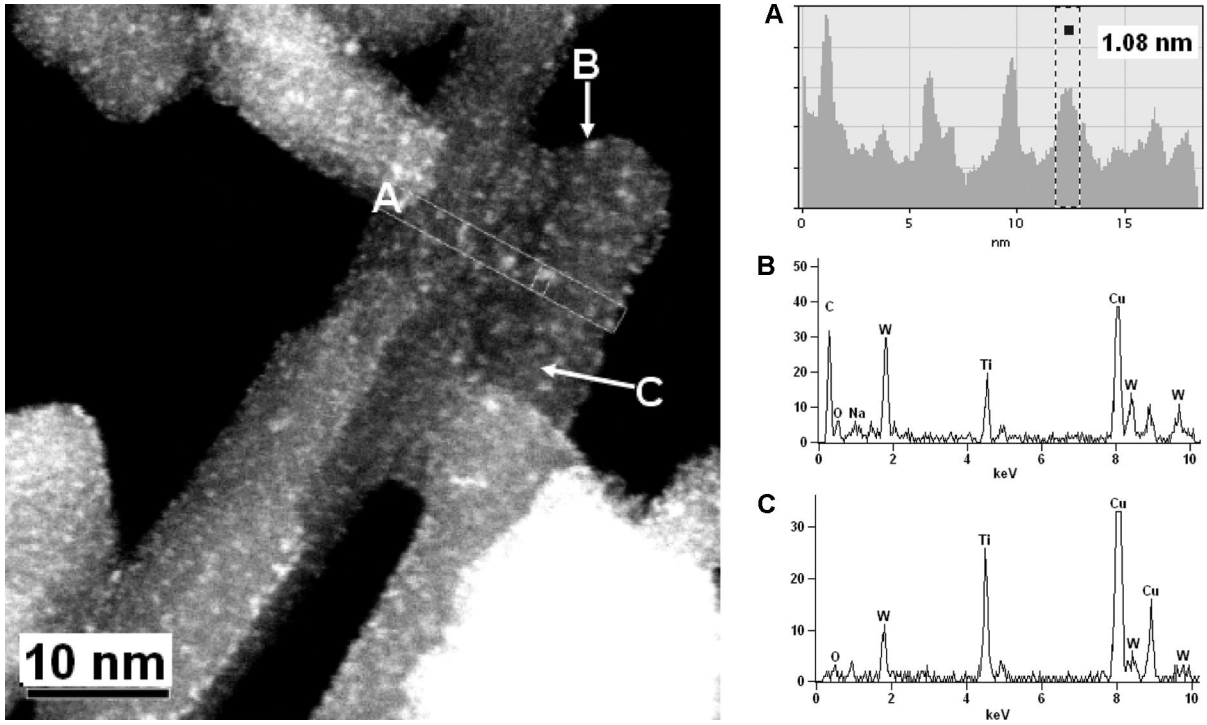

Figure 5. HAADF-STEM image of NTW-15 catalyst after annealing at 500 °C. Inset A: Intensity profile of white nanoparticles, marked as A in HAADF-STEM image. Inset B: EDXS analysis on white particles, marked as B in HAADF image. Inset C: EDXS analysis in dark region of nanorod particles.

3. Results and Discussion

3.1. Textural Properties. The NT support, after annealing at 400 °C, showed a decrease in textural properties as indicated in Table 1, where SSA decreased from 310 to 257 m^2/g, as a consequence of the conversion of the layered nanotubular structure into anatase domains on the walls, while maintaining the nanotubular morphology.[54] Normally, NT support, dried at 110 °C, contains a large amount of OH groups and H_2O on the surface and in the interlayer region. In a manner similar to that in hydrous zirconia supports,[15] NT was impregnated with a tungstate solution. After WO_x/NT materials were annealed at 500 °C, both SSA and total pore volume (TPV) dropped considerably, ~75 m^2/g and 0.36 cm^3/g, respectively, but average pore size increased about 2.5 times compared with that of the plain support with nanotubular morphology. The internal porosity of nanotubes (~6 or 7 nm) disappeared, producing nanoparticles or rodlike particles, where the pore diameter is defined by the external porosity created from interparticles' void space, as shown below in the TEM images. NTW-20 sample calcined at 400 °C, that is, before the nanotubular collapse, showed a SSA slightly lower than that in WO_x/Al_2O_3 (228 m^2/g) used as reference with similar W loading and annealed at 500 °C.

The real amount of W impregnated on hydrous titania nanotubes, as determined by AAS is shown in Table 1. As can be noticed, there is not significant variation between the nominal and real value. The W surface density (W atoms/nm^2) was determined taking into account the SSA and the real amount of W loaded, this value is reported in Table 1.

3.2. Structure and Morphology. XRD patterns of NT support calcined at 400 °C and those of tungstated samples after annealing at 500 °C are shown in Figure 1. Both NT and NTW samples showed a clear anatase structure, indicating that at this temperature, all the NT crystal phase collapsed and transformed into tetragonal anatase phase. In NTW samples, additional to the anatase diffraction lines, other diffraction peaks of lower intensity were detected, which matched well with the 12–0772 JCPDS card number corresponding to sodium tungsten oxide phase. Accordingly, in NT support, synthesized through an alkali hydrothermal treatment, there are some residual alkaline Na^+ ions in the interlayer region of NT.[55] When the nanotubular structure transforms into anatase, the Na^+ ions migrate to the surface and react with WO_x species to form Na_2WO_4 nanoparticles on the surface of anatase TiO_2.[56]

The Raman spectra of tungstated NTW samples, calcined at 500 °C, showed mainly anatase active modes at 144, 200, 400, 505, and 640 cm^{-1},[57] in agreement with XRD results. In order to detect tungstate's vibrations, the Raman spectra were magnified in the 800−1000 cm^{-1} region (see inset in Figure 2). A broadband at 935 cm^{-1} was observed for the higher W content samples, that is, NTW-15 and NTW-20, corresponding to the υ_1 symmetric vibration of tetrahedral W^{6+} cations.[36,58] In fact, in both samples, a weak peak at 924 cm^{-1} overlapped on the broad one, which corresponds

(54) Toledo-Antonio, J. A.; Capula, S.; Cortés-Jácome, M. A.; Angeles-Chavez, C.; López-Salinas, E.; Ferrat, G.; Navarrete, J.; Escobar, J. *J. Phys. Chem. C.* **2007**, *111*, 10799.

(55) Bavykin, D. V.; Friedrich, J. M.; Lapkin, A. A.; Walsh, F. C. *Chem. Mater.* **2006**, *18*, 1124.

(56) Cortes-Jácome, M.; Morales, M.; Angeles-Chavez, C.; López-Salinas, E.; Toledo Antonio, J. A. *J. Solid State Chem.* **2007**, *180*, 2682.

(57) Balachandran, U.; Eror, N. G. *J. Solid State Chem.* **1982**, *42*, 276.

(58) Nyquist, R. A.; Putziq, C. L.; Leugers, M. A. *Handbook of Infrarred and Raman Spectra of Inorganic Compounds and Inorganic Salts*; Academic Press: San Diego, 1997; Vol. 1, p 18.

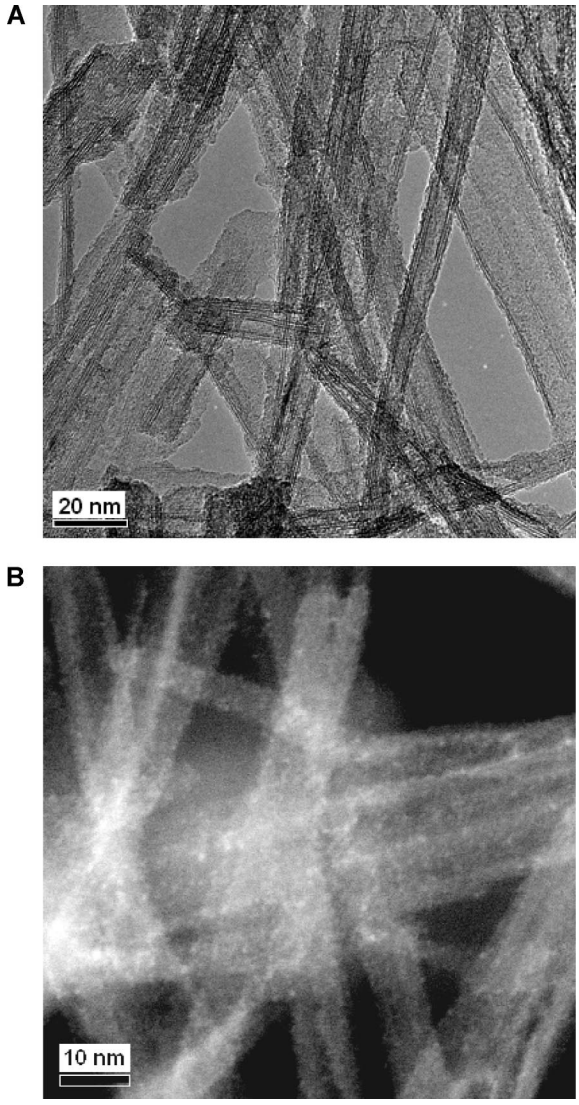

Figure 6. Electron microscopy of tungstate impregnated on titania nanotubes (NTW-20 after annealing at 400 °C). (a) TEM image and (b) HAADF-STEM image showing nanotubular features smeared by white WO_x nanoparticles.

to the bands of tetrahedrally coordinated W atoms in Na_2WO_4 compound.[59] It can then be concluded that all the W atoms are in tetrahedral coordination, even at high W concentration. Tetrahedral W species have been reported at low W loading[60] that transform into octahedral W species at higher concentration because of the polycondensation of the W species. In our case, the tetrahedral W atom coordination may be caused by the solid-state reaction of W atoms with Na^+ ions released during the partial collapse of the nanotubular structure. This phenomenon was studied in more detail in the sample with the highest W loading (e.g., NTW-20). Raman spectra of the sample calcined at 400 °C, that is, before collapse of the NT support, in comparison with the same sample annealed at 500 °C, where the nanotubular structure has broken apart, is shown in Figure 3. In the calcined material at 400 °C, Raman spectra showed a broadband at 964 cm^{-1} attributed to υ(W═O) in octahedral coordination.[61] In contrast, after calcining at 500 °C, υ(W═O) in a tetrahedral environment was observed at 934 and 924 cm^{-1}, originating from a solid-state reaction between WO_x and Na^+ ions.

In agreement with previous results, nanotubular features of NT support were maintained when annealing at 400 °C, as shown in images in Figure 4a. Although some short nanotubes were observed, the entire sample was composed of nanotubes of several micrometers long, with the outer and inner average diameters being 9.5 and 5.5 nm, respectively. As can be observed in the HRTEM images, the nanotube's walls are composed by at least two layers (see Figure 4b). After tungstate impregnation and annealing at 500 °C, nanotubular morphology completely collapsed, yielding nanorods and nanoparticles (see Figure 4c). In fact, in some regions, nanotubes have turned into large rodlike particles, and in some of these regions, these nanorods broke apart into smaller spherical nanoparticles. These features were more evident in the bright-field TEM image taken at higher magnification, as illustrated in Figure 4d.

Tungsten nanoparticles were not revealed by bright-field TEM image, and HAADF was then used to highlight the difference in contrast produced by tungsten in comparison with titanium and oxygen atoms, which are lighter elements. The result obtained is displayed in a HAADF-STEM image in Figure 5, showing rodlike particles dotted by a large amount of very small white particles. As the intensity in HAADF images depends on the atomic number, the small white particles are likely to be tungsten nanoparticles. The size of these WO_x nanoparticles was measured using the intensity profile of several white nanoparticles as shown in the A-region in Figure 5 and is included as an inset in the same figure. The size of one of the biggest white particles was 1.08 nm. Hence, WO_x particles dispersed on anatase TiO_2 are around 1 nm.

A confirmation that the white nanoparticles were made of tungsten atoms was provided through local chemical analysis of the white particles by the STEM-EDX technique. This technique allows a better control of the electron beam in order to acquire a local analysis of around 1 nm. The result obtained from the white nanoparticles is displayed in the EDX spectrum as inset B in Figure 5. The characteristic signals of tungsten atoms were intensely detected in the white particles; in contrast, the chemical analysis of the nanorods detected mainly Ti atoms, as presented in spectrum in inset C in Figure 5. Tungstated titania catalysts obtained by a nanotubular support precursor then lead to the formation of an anatase support decorated by ~1 nm WO_x nanoparticles, which may be active catalysts for oxidation reactions.

It is worth pointing out that NTW-20 sample calcined at 400 °C preserved the nanotubular morphology, as shown in Figure 6a, but the walls of the nanotubes appear homogeneously smeared by very small tungsten nanoparticles, which is highlighted by HAADF-STEM image in Figure 6b. Here, smaller white particles than those observed on the surface of rodlike particles (compare with Figure 5), can be observed. However, it is important to mention that tungsten coordina-

(59) Herrera, J. E.; Resasco, D. E. *J. Catal.* **2004**, *221*, 354.
(60) Vuurman, M. A.; Wachs, I. A.; Hirt, A. M. *J. Phys. Chem.* **1991**, *95*, 9928.
(61) Loridant, S.; Feche, C.; Essayem, N.; Figueras, F. *J. Phys. Chem. B* **2005**, *109*, 5631.

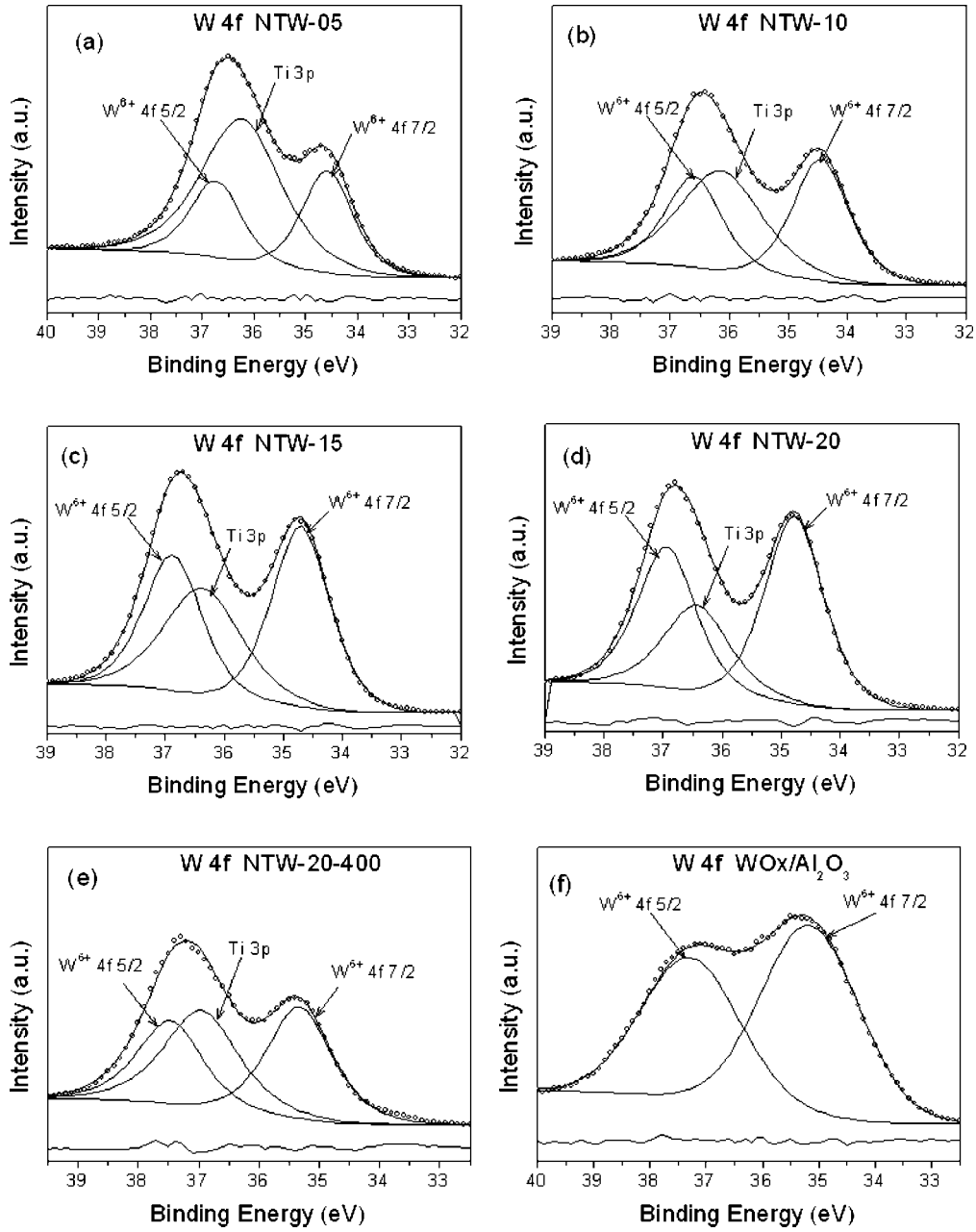

Figure 7. XPS spectra of W (4f) region overlapping with that of Ti(3p) in samples annealed at 500 °C. (a) NTW-05, (b) NTW-10, (c) NTW-15, (d) NTW-20, (e) NTW-20 annealed at 400 °C, and (f) WO_x/Al_2O_3.

Table 2. XPS Parameters of W ($4f_{7/2}$) and Ti ($2p_{3/2}$) on NTW-*x* Catalysts Annealed at 500 °C

	W^{6+} ($4f_{7/2}$)			Ti^{4+} ($2p_{3/2}$)			
catalyst	BE (eV)	fwhm (eV)	surface concentration (at %)	BE (eV)	fwhm (eV)	surface concentration (at %)	surface coverage W/(W+Ti)
NTW-05	34.6	1.2	2.26	457.9	1.1	38.08	0.056
NTW-10	34.5	1.2	3.18	457.9	1.0	34.25	0.085
NTW-15	34.7	1.2	4.74	458.1	1.0	33.79	0.123
NTW-20	34.8	1.2	5.95	458.3	1.0	33.47	0.151
NTW-20[a]	35.3	1.3	3.79	458.6	1.1	39.58	0.087

[a] Annealed at 400 °C.

tion changes from octahedral to tetrahedral with the change in the morphology of the support. Also, the concentration of these white tungsten nanoparticles on the surface of nanotubular support was smaller than that observed in anatase particles from a sample calcined at 500 °C, because of the higher SSA of the nanotubular support, suggesting that nanotubes are able to disperse a higher amount of WO_x nanoparticles on its surface. To the best of our knowledge, this is the first time that direct evidence of so-called isolated WO_x species deposited on a support at low W surface density (~3 W/nm^2) are given by HAADF-STEM (Figure 6).

3.3. Surface Chemical Composition. All the previous results were obtained by bulk-type characterization techniques, but a closer insight into surface-only species can be

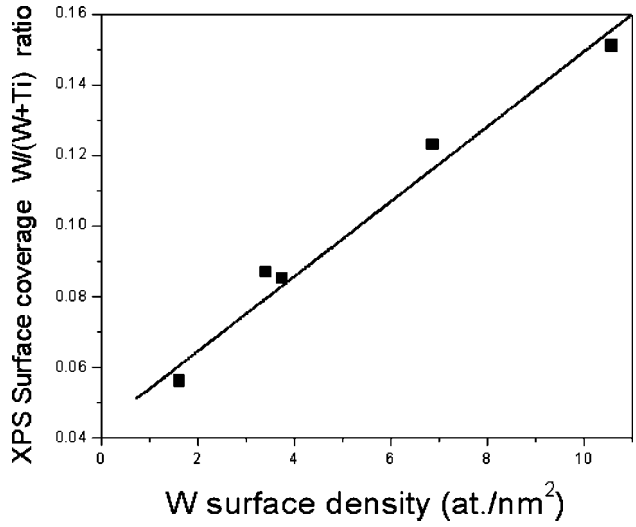

Figure 8. W surface density versus W surface coverage determined by XPS (W/W+Ti) atomic ratio.

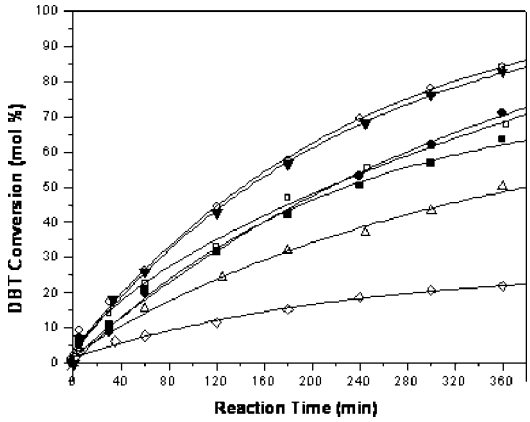

Figure 9. DBT conversion during ODS reaction on NTW-*x* catalysts annealed at 500 °C (○) NTW-20, (▼) NTW-15, (□) NTW-10, (Δ) NTW-05; (•) NTW-20 annealed at 400 °C, (◇) NT support annealed at 400 °C, (■) WO_x/Al_2O_3.

achieved by XPS spectroscopy. The XPS spectra of the NTW samples after calcination at 500 °C showed significant differences in the shape of the W (4f) + Ti (3p) region (see Figure 7). The W (4f) doublet of the NTW samples annealed at 500 °C showed an unusual asymmetry due to overlapping with the Ti (3p) component. The asymmetric shape of the W (4f) region was modified with the increase in overall W concentration and concomitant increase in surface tungsten concentration. In fact, in the sample with the same tungsten concentration annealed at 500 and 400 °C, panels d and e in Figure 7, the shape of the spectra varied as a consequence of a lower density of W atoms on the higher surface of the nanotubes. To quantify the amount of W atoms on the surface, the spectra at the W (4f) region were then fitted with one doublet and a single peak corresponding to Ti 3p, as reported elsewhere.[62] The BE value of the doublet was 34.6 ± 0.2 eV for the samples annealed at 500 °C, as indicated in Table 2. This value shifted to 35.3 ± 0.2 eV for the NTW-20 sample annealed at 400 °C. The shift observed in the BE of the W ($4f_{7/2}$) peak can be explained by the change observed in the coordination of W atoms in our Raman results (see Figure 3). According to literature data, in WO_x/ZrO_2 system, where all W atoms are in octahedral coordination, the BE values reported for W^{6+} and W^{5+} atoms are 35.5 ± 0.2 and 34.6 ± 0.3 eV, respectively.[43] In this case, in octahedrally coordinated W atoms, that is, NTW-20 annealed at 400 °C, the BE of W ($4f_{7/2}$) was 35.3 eV, corresponding to a W^{6+} oxidation state. When the NTW-20 sample was annealed at 500 °C, the BE of W ($4f_{7/2}$) decreased to 34.6 ± 0.2 eV because of the tetrahedral coordination of W atoms, not to a change in oxidation state such as in WO_x/ZrO_2 system.[28,29] The FHWM value of the W($4f_{7/2}$) peak was 1.2 eV, as indicated in Table 2, suggesting only one oxidation state of W atoms.

On the other hand, the spectra of Ti 2p region were fitted with just one doublet (see the Supporting Information). The BE value of the Ti ($2p_{3/2}$) signal was 458.0 ± 0.2 eV for the sample annealed at 500 °C, and this value shifted to 458.7 for NTW-20 annealed at 400 °C. All samples showed a FHWM value of 1.0 ± 0.1 eV, suggesting that only the Ti^{4+} oxidation state is present. The variation in the BE of Ti^{4+}, as in W atoms, can be related to a change in the symmetry of the Ti atoms from tetragonal anatase to orthorhombic layered nanotubular structure.[50]

Surface chemical composition was determined from W(4f) spectra by subtracting the Ti(3p) contribution and taking into account Ti (2p), O(1s), and Na(1s) spectra details. As expected, the W^{6+} surface concentration in Table 2 increased with W content in samples calcined at 500 °C, whereas the Ti^{4+} surface concentration decreased. On the NTW-20 annealed at 400 °C, the W surface concentration is lower when compared with the sample annealed at 500 °C; both samples have the same W loading, but the difference in surface WO_x concentration is attributed to the large surface area showed by the nanotubular support (see Table 1). In fact, WO_x surface coverage was determined by means of the (W/(W + Ti)) XPS surface atomic ratio presented in Table 2. WO_x surface coverage linearly correlates to the WO_x surface density, determined from the real W content and SSA of the samples, being independent of the annealing temperature, as shown in Figure 8. These results suggest that NT support is able to uniformly disperse the amount of W atoms loaded on its surface, and that the WO_x surface density reflects the WO_x surface composition.

3.4. Catalytic Activity. It is well-known that sulfur containing hydrocarbons can be oxidized to sulfones over tungsten containing catalysts using H_2O_2 or *tert*-butyl hydroperoxide as oxidants in different solvents, such as acetonitrile, γ-butyrolactone, butanol, etc.[35,36] Figueras et al.[36] reported that solids containing tetrahedral W cations deposited on ZrO_2 without calcination showed higher activity than those containing octahedrally coordinated W atoms in WO_3 clusters. In our study, WO_x species with either tetrahedral or octahedral coordination on titania support and an initial nanotubular morphology were applied as catalysts in the oxidation of DBT by H_2O_2. This reaction yields mainly the corresponding sulfone with 100% selectivity. The DBT

(62) Scholz, A.; Schnyder, B.; Wokaun, A. *J. Mol. Catal. A* **1999**, *138*, 249.

Table 3. Catalytic Activity in the Oxidation of DBT at 60 °C on Nanotubular TiO_2 Support and Tungstated Catalysts Annealed at 500 °C

sample	conversion[c] (mol %)	k_{app} (cm^3/(g min))	$(-r_0)_{DBT} \times 10^4$ (mol/(g min))	TOR $\times 10^3$ (1/s)
NT support	21.9	0.123	0.991	
NTW-05	50.1	3.519	2.003	15.5
NTW-10	67.9	5.947	3.201	11.9
NTW-15	82.7	9.346	4.135	8.5
NTW-20	84.1	9.877	3.968	5.5
NTW-20[a]	71.1	6.567	3.005	4.2
WO_x/Al_2O_3[b]	63.6	5.306	2.985	4.2

[a] Annealed at 400 °C. [b] 17.8 wt % of W atoms supported on alumina, used as reference. [c] At 360 min.

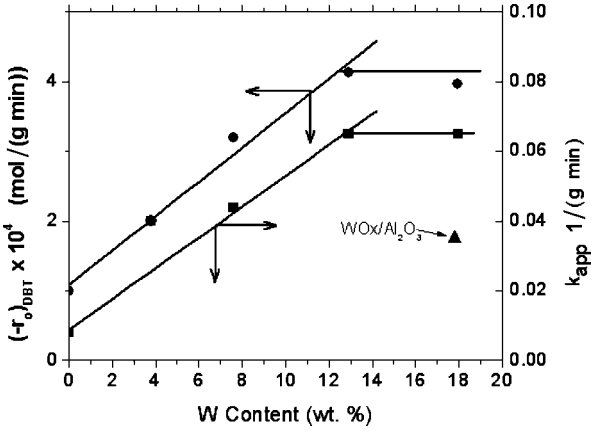

Figure 10. Initial reaction rate and kinetic apparent constant as a function of W concentration on NTW samples annealed at 500 °C. (▲) Kinetic apparent constant of WO_x/Al_2O_3 used as reference.

conversion attained with reaction time is shown in Figure 9. The NT support itself, annealed at 400 °C, is able to transform DBT into the sulfone; after 360 min of reaction, 21.9 mol % DBT was converted to the corresponding sulfone, as indicated in Table 3. The activity of the support can be explained by the oxidizing capacity intrinsic of the titanium atoms. In fact, titanium incorporated into microporous materials, such as zeolites (Ti-ZSM-12, Ti-Beta, TS-1) and mesoporous MCM-type titano-silicates (Ti-MCM-41 Ti-HMS), efficiently oxidize different organic substrates such as olefins, phenols, alcohols, thioethers, and sulfoxides.[39–43]

In tungstated NTW catalysts after annealing at 500 °C, DBT conversion increases with the W content, reaching a maximum in NTW-15 sample, as shown in Figures 9 and 10. At higher W content, for instance, in NTW-20 catalyst, similar conversion and apparent kinetic constant and initial reaction rate to the NTW-15 sample were obtained, as indicated in Table 3. This result points out that NTW-15 calcined at 500 °C with a W surface density around 6.9 W/nm^2 and a surface coverage [W/(W+Ti)] atomic ratio of 0.12 is the optimum W surface concentration to improve the oxidation of DBT reaction.

Correlations between initial reaction rate and WO_x surface coverage and WO_x surface density (W/nm^2) are plotted in Figure 11. The same dependence was observed between the reaction rate and XPS surface coverage and W surface density, as expected because of the linear correlation observed between these two parameters (see Figure 8). The rate increases linearly along both W surface coverage and

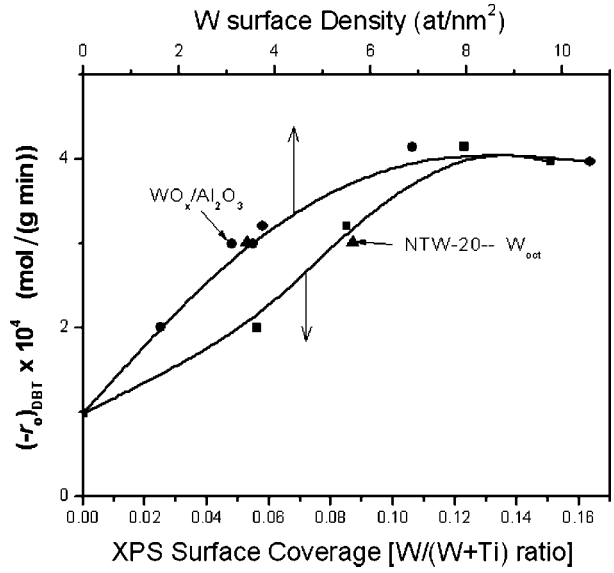

Figure 11. Specific reaction rate of oxidation of DBT as a function of W surface coverage determined by XPS and W surface density, determined from W concentration and SSA; catalysts from different supports annealed at 500 and 400 °C.

surface density, reaching a maximum at a surface coverage of 0.12, which represents a W surface density around 7 W/nm^2.

It is worth mentioning that in the nanotubular morphology, that is, NTW-20 catalyst annealed at 400 °C, W atoms are in octahedral coordination, as clearly identified in our Raman results in Figure 3. Tungsten nanoparticles were uniformly dispersed on the surface of nanotubes (see Figure 7), having practically the same W surface coverage and surface density as that in NTW-10 catalysts annealed at 500 °C showing similar initial reaction rates, 3.0×10^{-4} and 3.2×10^{-4} mol/(g min), respectively, as indicated in Figure 10 and Table 3. However, the NTW-20 annealed at 400 °C had higher SSA and W content than NTW-10 annealed at 500 °C. Therefore, a higher population of W sites in octahedral coordination should be present in NTW-20 annealed at 400 °C than in NTW-10 annealed at 500 °C. This result indicates that the oxidation of DBT reaction rate is not proportional to the number of W sites. A comparison with the reference catalyst, 17.8 wt % W on alumina annealed at 500 °C with a surface coverage of 0.08 and a W surface density of 3.1 W/nm^2 and with similar composition to NTW-20 annealed at 400 °C, was included in Table 3 and Figure 10. In the reference alumina catalyst, the reaction rate was 2.98×10^{-4} mol/(g min), quite similar to the rate of both NTW-10 and NTW-20 annealed at 400 °C, with similar W surface coverage and surface density. In a comparison of the reference catalyst with NTW-20 catalyst annealed at 500 °C, both with similar W concentration, but different W surface coverage and surface density, NTW-20 was more active than alumina catalyst. Hence, rather than the number of active sites, the oxidation of DBT reaction rate is strongly influenced by the WO_x surface coverage. Accordingly, a similar conclusion was reported for toluene isomerization rates in a WO_x/ZrO_2 system; the W surface density was modified by increasing the annealing temperature at a constant W

concentration or increasing W concentration at a constant annealing temperature.[15]

As the reaction rate was similar for NTW-10 catalyst (at 500 °C) containing tetrahedral W atoms and NTW-20 (at 400 °C) containing octahedral W atoms, with a higher amount of W sites, then the tetrahedral sites must be more active than the octahedral ones. To establish a more appropriate comparison, a normalization of the reaction rates by the total number of W atoms gives the turnover rates (TOR) of the different coordination environment of W atoms, which are included in Table 3. Catalysts with the same W surface coverage, NTW-20 (at 400 °C) and NTW-10 (at 500 °C), but with different coordination, showed quite different turnover rates, confirming that the tetrahedral coordination of W sites is more active than octahedral coordination.

The same result can be obtained by comparing the TOR of NTW-20 annealed at 400 and 500 °C, both with constant W content but different W surface coverage and different W coordination; the higher TOR activity was for the sample annealed at 500 °C, where the W atoms are in tetrahedral coordination. These results suggest that tetrahedral W coordination are twice as active as octahedral ones, confirming the earlier findings by Figueras et al. [36] in WO_x/ZrO_2 catalysts in which the W tetrahedral coordination was attained before calcination in dried samples. In our catalysts, both tetrahedral and octahedral coordination were obtained in samples calcined at 500 and 400 °C, respectively.

Finally, reference WO_x/Al_2O_3 was compared with NTW-20 annealed at 400 °C, with the same W content, surface coverage, and W coordination, showing the same TOR, as shown in Table 3. It can then be concluded that the support did not influence the activity of the W atoms in the oxidation of DBT.

4. Conclusions

Well-dispersed tungsten oxide on titania nanotubes were prepared by impregnation of nanotubular hydrous titania with ammonium metatungstate followed by annealing at 400 °C. At a higher annealing temperature, i.e., 500 °C, the nanotubular morphology of titania support collapsed and transformed into anatase, with a higher W surface density than the parent tungstated nanotubular precursor. The collapse of the nanotubular morphology releases residual Na^+ ions, initially located into the interlayer space of nanotubes walls, that react with W atoms, which change coordination from octahedral to tetrahedral as observed by Raman spectroscopy. XPS studies showed exclusively W^{6+} oxidation state with a surface coverage determined as W/(W+Ti) atomic ratio that linearly correlate with the W surface density independent of the annealing temperature.

The reaction rate of DBT oxidation increases linearly with W content in samples calcined at 500 °C, reaching a maximum at a W surface coverage around 0.12 as [W/(W+Ti)] atomic ratio, corresponding to a W surface density of 6.9 W/nm^2. The specific reaction rate depended strongly on the W surface coverage rather than on the number of W sites.

The turnover rates in the oxidation of DBT suggest that isolated W atoms in tetrahedral coordination are at least twice as active as octahedral ones. W atoms with octahedral coordination dispersed on alumina showed TOR quite similar to those with the same coordination dispersed on a nanotubular titania, suggesting no influence of the support on the oxidation of DBT reaction.

Acknowledgment. This work was financially supported by IMP Projects D.00237, D.00446, and I.00383.

Supporting Information Available: XPS spectra (PDF). This material is available free of charge via the Internet at http://pubs.acs.org.

CM702010K